Chemical Physics Letters 754 (2020) 137571

Contents lists available at ScienceDirect

Chemical Physics Letters

journal homepage: www.elsevier.com/locate/cplett

Research paper

Competition between interatomic Coulombic decay and autoionization of doubly-excited atoms

Ghazal Jabbari, Kirill Gokhberg, Lorenz S. Cederbaum*

Theoretische Chemie, Physikalisch-Chemisches Institut, Universität Heidelberg, Im Neuenheimer Feld 229, Heidelberg D-69120, Germany

HIGHLIGHTS

- Doubly-excited atoms can ionize a neighbor via ICD.
- ICD can dominate autoionization for higher doubly-excited states.
- Other interatomic processes can take place in environment.
- Amenable to experiment.

ABSTRACT

Doubly-excited atoms are known to autoionize. It is shown that in the presence of a neighboring atom, there is competition between autoionization and ICD (Interatomic Coulombic Decay) where the doubly-excited atom partially relaxes and the neighbor ionizes. Through a Rydberg series of doubly-excited states, the autoionization rate decreases in contrast to the ICD rate and ICD becomes dominant. Depending on the nature of the neighbor and the number of neighbors, other interatomic processes become operative even after autoionization, all demonstrating that the physics of doubly-excited species is strongly enriched in the presence of neighbors. Explicit examples are discussed.

Doubly-excited states of atoms are characterized by a high degree of electron correlation and the respective states of the helium atom have been fundamental to our understanding of this type of correlation. These states manifest themselves as resonances in the photoionization spectra and have been extensively investigated since the pioneering experimental work by Madden and Codling [1]. Nowadays they serve as prototype resonances to study autoionization. The excitation of two electrons to a discrete state and the consequent interaction of this state with the continuum results in the well-known asymmetric Fano peak in the photoionization spectrum [2]. In He, for instance, the first series of such autoionizing states with at least one electron in the n = 2 shell appears within 60–65 eV photon energy range, and have been studied in detail both theoretically and experimentally, see, e.g., [3–6]. A schematic picture of the double excitation of He by a single photon and the subsequent autoionization process is depicted in Fig. 1.

States comprised of two excited electrons are expected to be more sensitive to perturbation by the environment than those with a single excited electron. In a recent work by LaForge et al. the doubly-excited states of He are investigated in helium nanodroplets using synchrotron radiation [7]. Although the electron spectrum is qualitatively similar to the atomic one, the presence of weakly bound neighbors results in broadened and blueshifted peaks due to the perturbation caused by neighbors, and possibly environmental processes such as interatomic Coulombic decay [8]. In general, in condensed matter these structures tend to be unresolved or may even be washed out as the wave functions of the excited atoms are spatially extended and thus may experience strong perturbations by neighboring atoms.

Interatomic Coulombic decay (ICD) is an efficient decay channel in photoexcited systems, such as van der Waals and hydrogen bonded clusters and solutions. In the ICD process the de-excitation of a photoexcited atom or molecule and the energy transfer to the environment cause ionization of the environment through interatomic electronic correlation [9]. Since its prediction [8] ICD has been studied vastly, found to take place on the femtosecond timescale, and in most cases to be fast enough to quench concurrent electronic and nuclear mechanisms [10–13]. It becomes particularly fast when the intermolecular (interatomic) distances are small and the number of neighbors is large. This facilitates the energy transfer on the one hand and provides many open ICD channels on the other hand, causing relatively high ICD rates [14–17].

Here, we aim to investigate the competition between ICD and autoionization in doubly-excited Rydberg states of helium in an

* Corresponding author.
E-mail addresses: kirill.gokhberg@pci.uni-heidelberg.de (K. Gokhberg), Lorenz.Cederbaum@pci.uni-heidelberg.de (L.S. Cederbaum).

https://doi.org/10.1016/j.cplett.2020.137571
Received 9 March 2020; Received in revised form 2 May 2020; Accepted 4 May 2020
Available online 20 May 2020

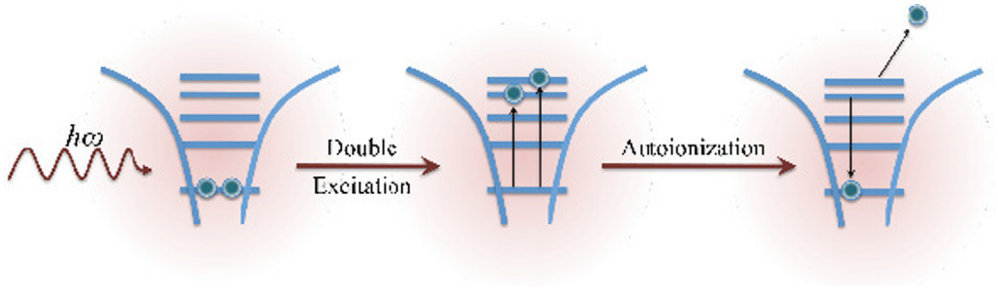

Fig. 1. Schematic picture of the double excitation of an isolated He atom by a single photon and the subsequent autoionization process.

environment of neon atoms. First, we concentrate on the HeNe dimer where our main goal is to compute *ab initio* the respective rates for the low lying states He**(2s2p) Ne and He**(23sp+) Ne and to discuss semi-quantitatively the situation in higher doubly-excited states. For the former states the autoionization rates are large and become smaller for the latter. Then, we would like to touch upon the presence of more Ne neighbors.

We would like to stress that the HeNe dimer has been studied before experimentally and theoretically in the context of ICD [18,19]. In these interesting contributions vibrationally resolved ICD has been explored in detail after single photo-excitation of He. The He atom is thereby always bound below the He ionization threshold. In the present work the doubly-excited He is autoionizing and there is a competition with ICD. A schematic picture of the double excitation of He in the HeNe dimer by a single photon and the subsequent ICD process is depicted in Fig. 2.

Before addressing HeNe, let us discuss the doubly excited isolated Helium atom which is a prototype system to study autoionization. There are many theoretical and experimental works on the optically allowed $^1P^0$ double excitation of He atom, see, for instance, [3,4]. The first member of $^1P^0$ family is the 2*s*2*p* excitation which corresponds to a peak in the photoionization spectrum of the He atom at photon energy 60.1503 eV. Its autoionization decay width is 37.6 meV correspondig to a short lifetime of 17.5 fs. This state is the first member of both 2*s*, *np* and *ns*, 2*p* Rydberg series, where the *inner* excited electron is in the n = 2 shell, and the *outer* electron is in the n = 2,3,4,…shells. The energies of these excitations varies between 60 to 65.4 eV.

The 2*s*, *np* and *ns*, 2*p* series mix strongly and they contribute to two different Rydberg series of (2*nsp* +) and (2*nsp* −). The + and − signs stand for addition and subtraction of the wave functions Ψ(2*p*, *ns*) and Ψ(2*s*, *np*) [3]. The optical transitions from the ground state to − levels are quasi-forbidden and, hence, one observes only He**(2*nsp*+) peaks in the experiment. The next member of the optically allowed Rydberg series is He**(23*sp*+) which appears in the spectrum at 63.6575 eV photon energy and exhibits a decay width of 8.3 meV (79.3 fs) [3,4].

We have computed the decay widths of the above mentioned two resonances using the method discussed below for the calculations on HeNe and obtained 39.4 meV and 8.2 meV, respectively. The error is within the expected range of the method.

We now turn to HeNe. The ground state potential energy curve has been reported in the literature [20,19]. The dimer was found to be bound in its electronic ground state by 1.8 meV and to posses an equilibrium distance of R_{eq} = 3.035 Å. To proceed we have computed the potential energy curves of the decaying states and, most importantly, also the respective decay widths as a function of the internuclear separation R. To compute the energies we employed the ADC(2)x method for the polarization propagator [21,22], see below. In the *ab initio* calculations we used the cc-pVQZ basis set [23] on both atoms. The basis sets were augmented by four s, three p and two d even-tempered functions (β = 2.5) on He and by three s, two p and one d even-tempered functions (β = 2.5) on Ne. The MOLCAS 7.4 package [24] was employed for the *ab initio* calculation of Hartree-Fock energies and two-electron integrals needed as input data for the ADC calculations.

To calculate the autoionization and ICD widths for the HeNe dimer, we employed the Fano-ADC-Stieltjes method [21,25] and used the ADC(2)x in all the calculations. To compute the relevant matrix elements one has to select the configurations contributing to the initial and to the final states of the decay in question. Since the resonances correspond to doubly-excited states, the selection of configurations also extends to the doubly-excited, i.e., two-hole two-particle 2*h*-2*p*, configurations making the calculation rather cumbersome. To obtain the discrete parts of the Fano resonances we need to include all 2*h*-2*p* configurations where the holes are located on the He atom and remove the 1*h*-1*p* block from the ADC calculations. The calculations are then as for bound discrete states. For describing autoionization and ICD separately, different selection is clearly needed for the description of the final states of the decay. To calculate the partial rate of each process separately, the final state configurations have to be separated as well. In the case of the autoionization process, all 1*h*-1*p* configurations with the hole on the He atom must be included. In the case of ICD, however, the final state configurations are 2*h*-2*p* where the two final holes are located on different atoms, here, the helium and neon atoms. Once the selection of configurations has been done, we fully diagonalized the resulting ADC(2)x matrices to obtain the discrete part of the resonances and the vectors of the final states needed to calculate the rates via the Fano-ADC-Stieltjes method [21,25].

The computed potential energy curves (PECs), the autoionation (AI) and ICD widths for the doubly excited electronic states of HeNe emerging from He**(2*s*2*p*) and He**(23*sp*+) are depicted in Fig. 3 as a function of the internuclear distance. The PECs of all of the excited states indicate a rather strong binding and exhibit minima at around 1.8 Å. At the equilibrium geometry of HeNe the curves are already flat and close to the respective atomic energies. Each of the two He** states

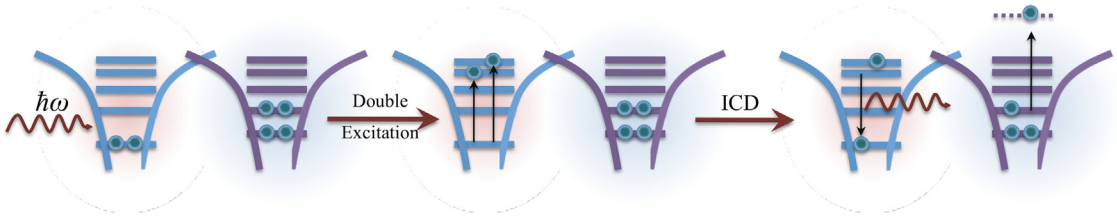

Fig. 2. Schematic picture of the double excitation of He atom in the HeNe dimer by a single photon and the subsequent ICD process.

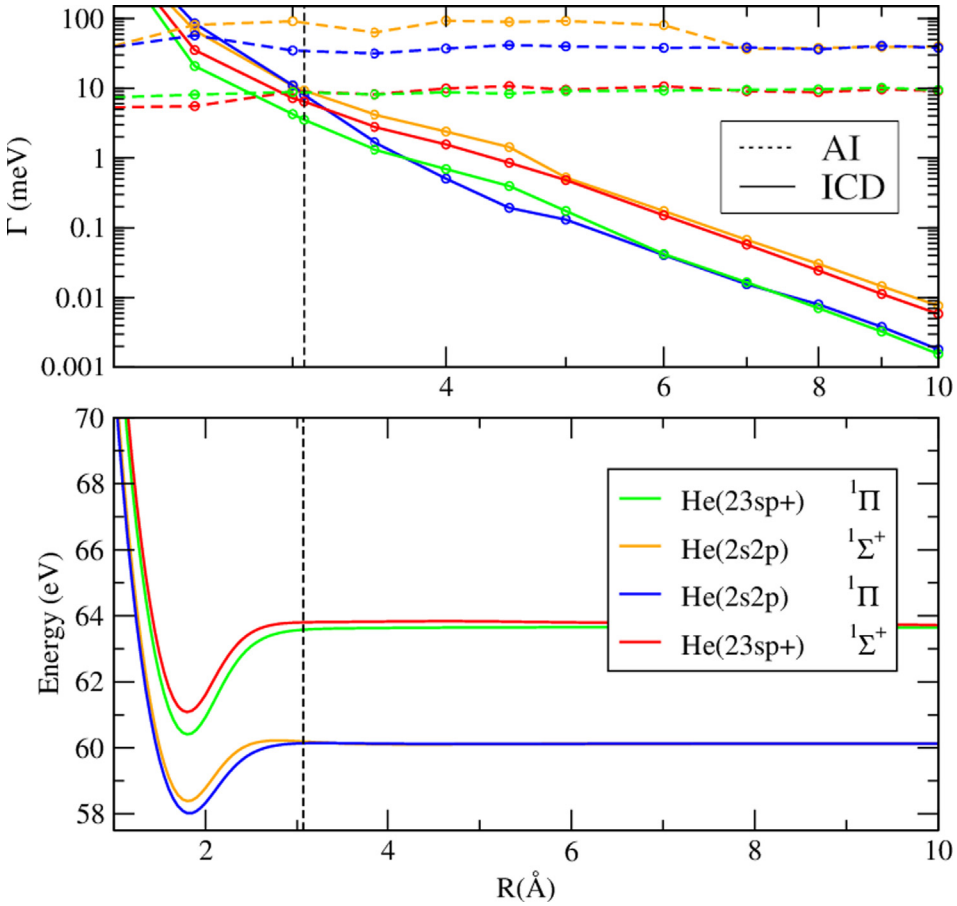

Fig. 3. Lower Panel: PECs of the doubly excited He atom in HeNe dimer. The total energy of the ground state atoms is chosen as the zero of the energy scale. The vertical dashed line at R = 3.01 Å denotes the position of the equilibrium geometry in the ground state of HeNe. Upper panel: The autoionization (dashed lines) and ICD widths (full lines) for the corresponding excited states. The logarithmic scale on both axes is chosen to illustrate the R dependence of the ICD width.

combined with Ne in the ground state gives rise to a $^1\Sigma^+$ and a $^1\Pi$ state. While the energies of such a pair are very similar to each other, the AI and ICD rates are rather different. The AI widths fall into two groups merging at large R into the known atomic AI widths of He**(2*s*2*p*) and He**(23*sp*+), respectively. At shorter distances, one can see in Fig. 3 the influence of the neighbor Ne. Also the ICD widths group in pairs at large R, but, in contrast, now the pairs are $^1\Sigma^+$ and $^1\Pi$, respectively. ICD rates are known to depend on the symmetry of the decaying state even at large R [26]. This is due to the fact that the electronic wavefunctions of the excited atom may or may not point towards the neighbor. The ICD rates are larger for the $^1\Sigma^+$ states.

The calculated AI and ICD widths at the equilibrium distance of HeNe are collected in Table 1. The influence of the Ne neighbor on the AI is surprisingly large for the $^1\Sigma^+$ He(2*s*2*p*) Ne state. For this state, the ICD rate is a little more than 10% of this rather large AI rate. For the other states, the ICD starts to become competitive with the AI, in particular for the $^1\Sigma^+$ He(23*sp* +) Ne state where ICD is 70% of the AI rate. Interestingly, the ICD widths can be even larger than the AI ones at short internuclear distances. This should manifest itself in experiment.

Table 1
Autoionization and ICD widths of HeNe dimer computed at equilibrium geometry. The autoionization widths computed with the same method (see text) are also given.

Molecular State	Isolated He atom AI width (meV)	AI width at eq HeNe dimer (meV)	ICD width at eq HeNe dimer (meV)
$^1\Sigma^+$ He(2*s*2*p*) Ne	39.4(5)	89.7(9)	9.3(0)
$^1\Pi$ He(2*s*2*p*) Ne	39.4(5)	32.6(5)	8.0(2)
$^1\Sigma^+$ He(23*sp* +) Ne	8.1(6)	8.9(5)	6.4(5)
$^1\Pi$ He(23*sp* +) Ne	8.1(6)	8.8(1)	3.5(2)

Once the HeNe dimer absorbs a photon leading to a doubly excited He, we encounter an essentially vertical excitation from the HeNe vibrational ground state to the states shown in Fig. 3 populating via the Frank-Condon principle the bound vibrational as well as the dissociative continuum of these electronic states. A glance at the figure tells us that the ICD widths in the R range of the bound vibrational states are even exceeding those of the AI widths.

Let us now discuss higher doubly-excited states. Since the correlation between the excited electrons occupying higher Rydberg orbitals becomes weaker, the autoionization rates are known to decrease [1,3–6]. To better understand the behavior of ICD for the higher doubly-excited states, we take recourse to the asymptotic expression for the partial ICD decay width valid for large R [27–29]

$$\Gamma_f = \frac{3\hbar}{4\pi}\left(\frac{c}{\omega}\right)^4 \frac{A_{i,f}\sigma^B}{R^6}, \quad (1)$$

where $A_{i,f}$ is the Einstein coefficient, i.e., inverse radiative lifetime, for the transition from the initial doubly-excited state *i* to the final state *f* of our system, here He, *c* is the speed of light, ω is the excess energy available for ionizing the neighbor, and σ^B is the photoionization cross section of the neighbor, here Ne, at this energy commonly called virtual photon energy. If the initial state can decay by ICD via more than one channel *f*, then the total decay rate is simply given by the sum over the partial widths $\Gamma = \sum_f \Gamma_f$. The above expression is for randomly oriented system and neighbor, but this suffices for our discussion of trends below.

Intuitively, the ICD rate increases with increasing photoionization cross section of the neighbor and decreases with growing excess energy. Counter intuitively, the shorter the radiative lifetime of the system is, the larger is the ICD rate. Clearly, the ICD rate is particularly sensitive to the excess energy and to the distance R at which the neighbor is

located.

The above relation is valid at distances R at which the overlap of the wavefunctions of the excited system (He**) and of the neighbor (Ne) is negligible. The overlap depends on the state of the system. In Fig. 3 we see that this is the case above about 6 Å where the *ab initio* rates merge into the $1/R^6$ behavior. Here, we are more interested in the ICD at the equilibrium R where the Eq. (1) is approximate. Being a lower bound to the exact rate [27,29], this approximation is very useful in estimating the true rates and in investigating trends.

The rate in Eq. (1) can be calculated using available experimental and computed data for the separated atoms. Absolute photoionization cross sections for rare gases are well known (see, e.g., [30]), radiative rates of doubly-excited states of He are reported in [6] and the energies of singly-excited states of He are tabulated in [31]. The latter are needed to calculate the excess energy and hence also the energy of the ICD electron emitted from the neighbor Ne. Radiative rates are known for final states of s and d symmetry and radiative decays that involve the change of both principal quantum numbers are much smaller [6].

The ICD widths computed with Eq. (1) and the above atomic data provide lines which are parallel to the $1/R^6$ tails at large R shown in Fig. 3. For the state He($2s2p$) Ne it is found that the asymptotic equation gives a value of about 3.2 times smaller than the *ab initio* value for the $^1\Pi$ state. Given that doubly excited states in a dimer are rather complicated to compute, and that the analytic expression is for randomly oriented system and neighbor, the agreement is acceptable. It is known that due to orientation of the excited state, its ICD rate is larger for $^1\Sigma^+$ states by up to a factor of 4 at large distances [32]. At equilibrium distance, as expected, the width computed with the asymptotic expression is 0.75 meV and thus about an order of magnitude smaller than the lowest *ab initio* value.

Let us compare the ICD widths for He($2s2p$) Ne and He($23sp+$) Ne. For large R we notice in Fig. 3 that both these states give essentially the same value ($^1\Pi$ and $^1\Sigma^+$ states must be considered separately due to symmetry). Can this surprising finding be understood from the asymptotic expression? The leading term in the ICD decay of these states is

$$He(2s2p)Ne \rightarrow He(1s2s)Ne^+ + e_{ICD}, \qquad (2)$$

$$He(23sp+)Ne \rightarrow He(1s3s)Ne^+ + e_{ICD},$$

providing excess energy, i.e., the difference between the energies of the doubly-excited state and the final singly-excited state of He, of 39.535 eV and 40.737 eV for 2s2p and 23sp+, respectively. Analogous results are obtained for the d-channel. The overall radiative rate of the latter doubly-excited state is slightly larger than that of the former making the total ICD widths rather similar for both states: 0.75 meV versus 0.69 meV.

We now turn to the competition between autoionization and ICD for doubly-excited states of higher members of the Rydberg series 2nsp+ and of 2nsp− where the *ab initio* computations become more cumbersome. The experimental atomic AI widths drop through a series. For 2s2p, 23sp + and 24sp+ of the AI widths are 37.6, 8.3, 3.4 meV [5], respectively, and continue to drop to 0.6 meV for 27sp+ [6]. As the excess energies converge in each series and the radiative rates keep growing slightly through the series [6], the ICD widths stays approximately constant (0.7 meV) in the 2nsp+ series. The situation is even more in favor of ICD for the 2nsp− Rydberg series. Here, the AI widths are 0.11, 0.06 and 0.03 meV for 23sp−, 24sp− and 25sp− [5] and continue to drop down for higher members [6]. As above, the excess energies do not change much and the radiative rates continuously grow along the series. The ICD widths are 0.56, 0.71 and 0.75 meV for the above states and strongly dominate the autoionization and thus control the whole decay process. It is interesting to investigate whether for dipole-forbidden doubly-excited states, ICD strongly dominates autoionization in general.

The competition between AI and ICD in doubly-excited states is, of course, not restricted to He. Doubly-excited states exist in many systems and have been investigated, in particular, in rare gas atoms, see, e.g., [33–35]. From the point of view of Eq. (1), other pairs than HeNe studied here, look more favorable. Other rare gas atoms than He have lower excess energies and suitable neighbors may have larger photoionization cross sections at these virtual photon energies. In Fig. 4 the cross sections of He, Ne, and Ar atoms are depicted as a function of photon energy. One can compare the cross sections at energies corresponding to the excitation energies we have chosen.

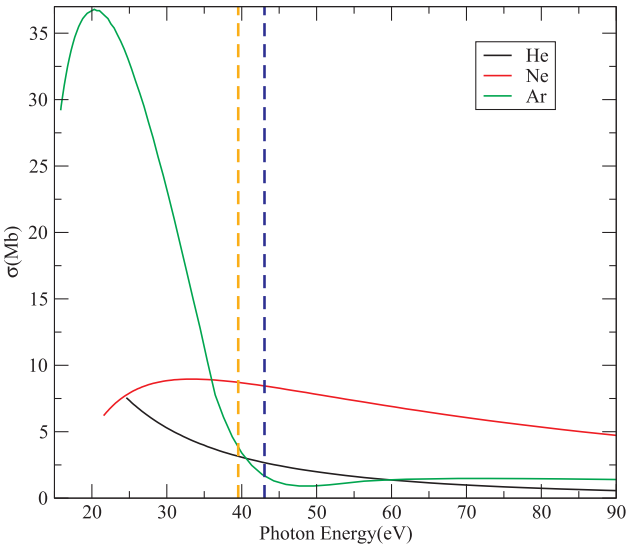

Fig. 4. Experimental values of absolute photoionization cross section for He, Ne, and Ar atom in the VUV spectral regions. The data for plotting the curves is taken from [30]. Dashed lines show the energy of the virtual photon absorbed by the neighboring atom in the ICD process for He(2s2p) (orange) and He(23sp+) (blue) and of N.e(3s3p) (black). (For interpretation of the references to color in this figure legend, the reader is referred to the web version of this article.)

It is clear that Ne is a suitable candidate as a neighbor for doubly-excited He. If we investigate doubly-excited Ne as our autoionizing system, Ar as a neighbor is particularly suitable from the point of view of a large photoionization cross section. The doubly-excited Ne**($3s3p$) lowest in energy is at 44.97 eV excitation energy [33] and the energy of the multiplet of singly-excited Ne*($3s$) is around 16.85 eV [31]. The excess energy is thus 28 eV and fits very well to Ar as a neighbor, see Fig. 4. The equilibrium distance between Ne and Ar is 3.5 Å[33] and if we assume that the radiative rate of Ne**($3s3p$) is similar to that of He**($2s2p$), we obtain an ICD width of 4.3 meV employing the asymptotic relation (1). Remembering that this value is a strong lower bound to the true ICD width, we may conclude that in NeAr ICD is competitive with AI (10 meV [33]) even for the lowest doubly-excited resonance.

As we have seen for doubly-excited He, the AI rates decrease substantially through the Rydberg series and this applies also to other rare gas atoms. The situation is similar in the case of inner-valence singly-excited rare gas atoms [33,36]. We have seen above that the ICD rates of doubly-excited atoms with a neighbor do not necessarily decrease as is also the case for the rates of ICD of inner-valence singly-excited rare gas atoms [37,38]. In Ne dimers, for example, it has been found that ICD is dominant over resonant Auger for inner-valence excitations to n>5 [37,38]. Inspection of the asymptotic relation (1) shows that this is due to the very different behavior of the radiative rates of doubly- and singly-excited atoms. As seen in [6], the radiative rates of doubly-excited He do not decrease through the Rydberg series. The relatively large radiative rates of doubly-excited states also play an important role in the absorption spectrum in the photon region of doubly-excited He [39].

The competition of AI and ICD of doubly-excited systems may

become even more intricate in the presence of more than one neighbor. The number of of ICD channels grows and hence also the ICD rate [17,40]. For N equivalent neighbors one can expect an enhancement of the ICD rate by N, at least in the asymptotic regime. In addition, dipole forbidden transitions of isolated atoms become more allowed due to interactions with neighbors and this may enrich the absorption spectrum [7] and also enhance the ICD rates [27]. There are other fascinating aspects of doubly-excited systems in environment. After ICD takes place as discussed in this work, the system is still singly-excited, see, for instance, Eq. (2). Let us consider He($23sp$ +)Ar_2 as an example. After ICD we have He($1s3s$) Ar^+Ar and the resulting He($1s3s$) possesses sufficient excess energy for a second ICD step to obtain He($1s^2$) Ar^+Ar^+ in spite of the Coulomb repulsion between the two Ar ions. This sequential double ICD will give rise to a Coulomb explosion [9].

If the first step of the relaxation of a doubly-excited state in environment is not ICD, but rather autoionizaion, another follow up interatomic process can take place. As explicit examples, let us consider HeMg, $HeMg_2$, and He at organic molecules after double-excitation of the He. Once autoionization of He occurs, He^+ is created. Now, ETMD (electron transfer mediated decay) can take place [41–44]. In contrast to ICD where only energy is transferred, ETMD involves the transfer of an electron. In the present case, a neighbor donates an electron to neutralize the He^+ ion and another electron is emitted from the same or another neighbor. After photo-double-excitation of He, the doubly-excited He** can undergo AI emitting an electron and producing a He^+ ion. This ion undergoes ETMD with the neighbors provided that the double ionization potential of the neighborhood is smaller than the ionization potential of He. For instance, the energy gain by neutralizing He^+ is 24.587 eV and the double ionization potential of Mg is 22.7 eV [31], thus giving

$$HeMg \rightarrow He(2s2p)Mg \rightarrow He^+Mg + e_{AI}, \quad (3)$$

$$He^+Mg \rightarrow He(1s^2)Mg^{++} + e_{ETMD}.$$

The ETMD process, i.e., the last line in Eq. (3), has been studied in detail theoretically for HeMg [45] and experimentally for $HeMg_2$ and larger Mg clusters [46]. In the latter case, one can find two Mg^+ ions as products. We would like to briefly mention that the probability to produce the dication via the ETMD is usually much higher than by direct single-photon double ionization [45,46].

Concerning organic molecules as neighbors, we notice that the double ionization potentials of aromatic molecules like naphtalene (21.39 eV), anthracene (20.07 eV), or larger polyacenes (<19 eV) [47] are smaller than the neutralization gain of He^+ or even Ne^+. Since these systems can accommodate several (up to 16) He atoms [48,49], the total photo-double-excitation cross section of He is enlarged in such microclusters and the process indicated in Eq. (3) is likely. In principle, doubly exciting Ne instead of He can also lead to the above process for these systems and the neutralization gain (21.565 eV [31]) is sufficiently large.

In conclusion, the presence of a neighboring atom to a doubly-excited atom leads to a competition between autoionization and ICD, where ICD becomes more favorable through the Rydberg series. Depending on the neighbor, an interesting ETMD process occurs after the autoionization of the doubly-excited atom neutralizing the resulting ion. If several neighbors are present, the ICD rate can be enhanced substantially, and, in addition, a sequential ICD step can become possible. All these phenomena call for experiments. Measuring the distribution of the emitted electrons provides unique information on the processes at hand. Since it has been demonstrated that measuring photons in coincidence with emitted electrons is a very useful tool to identify ICD [50,51], this technique can also be applied here, for example, to identify the radiation from the ICD product He($1s3s$) Ne^+ in Eq. (2).

Declaration of Competing Interest

The authors declare that they have no known competing financial interests or personal relationships that could have appeared to influence the work reported in this paper.

Acknowledgements

The authors thank A.I. Kuleff, C.D. Lin and M. Pernpointner for valuable contributions. Financial support by the European Research Council (ERC) (Advanced Investigator Grant No. 692657) is gratefully acknowledged

References

[1] R.P. Madden, K. Codling, Phys. Rev. Lett. 10 (1963) 516.
[2] U. Fano, Phys. Rev. 124 (1961) 1866.
[3] J.W. Cooper, U. Fano, F. Prats, Phys. Rev. Lett. 10 (1963) 518.
[4] K. Schulz, G. Kaindl, M. Domke, J.D. Bozek, P.A. Heimann, A.S. Schlachter, J.M. Rost, Phys. Rev. Lett. 77 (1996) 3086.
[5] Topical-Review: J.M. Rost, K. Schulz, M. Domke, G. Kaindl, J. Phys. B 30 (1997) 4663.
[6] C.-N. Liu, M.-K. Chen, C. Lin, Phys. Rev. A 64 (2001) 010501(R).
[7] A.C. LaForge, D. Regina, G. Jabbari, K. Gokhberg, N.V. Kryzhevoi, S.R. Krishnan, M. Hess, P. O'Keeffe, A. Ciavardini, K.C. Prince, R. Richter, F. Stienkemeier, L.S. Cederbaum, T. Pfeifer, R. Moshammer, M. Mudrich, Phys. Rev. A 93 (2016) 050502(R).
[8] L.S. Cederbaum, J. Zobeley, F. Tarantelli, Phys. Rev. Lett. 79 (1997) 4778.
[9] T. Jahnke, J. Phys. B 48 (2015) 082001.
[10] T. Jahnke, H. Sann, T. Havermeier, K. Kreidi, C. Stuck, M. Meckel, M. Schöffler, N. Neumann, R. Wallauer, S. Voss, A. Czasch, O. Jagutzki, A. Malakzadeh, F. Afaneh, T. Weber, H. Schmidt-Böcking, R. Dörner, Nat. Phys. 6 (2010) 139.
[11] M. Förstel, T. Arion, U. Hergenhahn, J. Electron. Spectrosc. Relat. Phenom. 191 (2013) 16.
[12] S. Kopelke, Y.-C. Chiang, K. Gokhberg, L.S. Cederbaum, J. Chem. Phys. 137 (2012) 034302.
[13] G. Jabbari, K. Sadri, L.S. Cederbaum, K. Gokhberg, J. Chem. Phys. 144 (2016) 164307.
[14] G. Öhrwall, N. Ottosson, W. Pokapanich, S. Legendre, S. Svensson, O. Björneholm, J. Phys. Chem. B 114 (2010) 17057.
[15] V. Stumpf, K. Gokhberg, L.S. Cederbaum, Nat. Chem. 8 (2016) 237.
[16] V. Stumpf, C. Brunken, K. Gokhberg, J. Chem. Phys. 145 (2016) 104306.
[17] R. Santra, L.S. Cederbaum, Phys. Rep. 368 (2002) 1.
[18] F. Trinter, J.B. Williams, M. Weller, M. Waitz, M. Pitzer, J. Voigtsberger, C. Schober, G. Kastirke, C. Müller, C. Goihl, P. Burzynski, F. Wiegandt, R. Wallauer, A. Kalinin, L.P.H. Schmidt, M.S. Schöffler, Y.-C. Chiang, K. Gokhberg, T. Jahnke, R. Dörner, Phys. Rev. Lett. 111 (2013) 233004.
[19] G. Jabbari, S. Klaiman, Y.-C. Chiang, F. Trinter, T. Jahnke, K. Gokhberg, J. Chem. Phys. 140 (2014) 224305.
[20] S.M. Cybulski, R.R. Toczylowski, J. Chem. Phys. 111 (1999) 10520.
[21] S. Kopelke, K. Gokhberg, V. Averbukh, F. Tarantelli, L.S. Cederbaum, J. Chem. Phys. 134 (2011) 094107.
[22] J. Schirmer, A.B. Trofimov, J. Chem. Phys. 120 (2004) 11449.
[23] B.P. Pritchard, D. Altarawy, B. Didier, T.D. Gibson, T.L. Windus, J. Chem. Inf. Model. 59 (2019) 4814.
[24] F. Aquilante, L. De Vico, N. Ferrè, G. Ghigo, P.-A. Malmqvist, P. Neogrády, T.B. Pedersen, M. Pitoňák, M. Reiher, B.O. Roos, L. Serrano-Andrés, M. Urban, V. Veryazov, R. Lindh, J. Comput. Chem. 31 (2010) 224.
[25] V. Averbukh, L.S. Cederbaum, J. Chem. Phys. 125 (2006) 094107.
[26] K. Gokhberg, N.V. Kryzhevoi, P. Kolorenc, and L.S. Cederbaum, Phys. Rev. A 81 (2010) 013417.
[27] V. Averbukh, I.B. Müller, L.S. Cederbaum, Phys. Rev. Lett. 93 (2004) 263002.
[28] K. Gokhberg, A.B. Trofimov, T. Sommerfeld, L.S. Cederbaum, Euro. Phys. Lett. 72 (2005) 228.
[29] L.S. Cederbaum, Phys. Rev. Lett. 121 (2018) 223001.
[30] G. Marr, J. West, At. Data Nucl. Data Tables 18 (1976) 497.
[31] A. Kramida, Y. Ralchenko, J. Reader, NIST-ASD-Team, NIST Atomic Spectra Database, 2019.
[32] K. Gokhberg, S. Kopelke, N.V. Kryzhevoi, P. Kolorenc, L.S. Cederbaum, Phys. Rev. A 81 (2010) 013417.
[33] K. Codling, R.P. Madden, D.L. Ederer, Phys. Rev. 155 (1967) 26.
[34] E. Bolduc, J.J. Quemener, P. Marmet, J. Chem. Phys. 57 (1972) 1957.
[35] J.T. Grissom, W.R. Garrett, R.N. Compton, Phys. Rev. Lett. 23 (1969) 1011.
[36] S. Sorensen, T. Aberg, J. Tulkki, E. Rachlew-Kaelne, G. Sundstrom, M. Kirm, Phys. Rev. A 50 (1994) 1218.
[37] S. Barth, S. Joshi, S. Marburger, V. Ulrich, A. Lindblad, G. Ohrwall, O. Bjornholm, U. Hergenhahn, J. Chem. Phys. 122 (2005) 241102.
[38] K. Gokhberg, V. Averbukh, L.S. Cederbaum, J. Chem. Phys. 124 (2006) 144315.
[39] J.E. Rubensson, C. Sathe, S. Cramm, B. Kessler, S. Stranges, R. Richter, M. Alagia, M. Coreno, Phys. Rev. Lett. 83 (1999) 947.
[40] G. Ohrwall, M. Tchaplyguine, M. Lundwall, R. Feifel, H. Bergersen, T. Rander,

A. Lindblad, A. Schulz, S. Peredkov, S. Barth, S. Marburger, U. Hergenhahn, S. Svensson, O. Bjornholm, Phys. Rev. Lett. 93 (2004) 173401.
[41] J. Zobeley, R. Santra, L.S. Cederbaum, J. Chem. Phys. 115 (2001) 5076.
[42] K. Sakai, S. Stoychev, T. Ouchi, I. Higuchi, M. Schoffler, T. Mazza, H. Fukuzawa, K. Nagaya, M. Yao, Y. Tamenori, A.I. Kuleff, N. Saito, K. Ueda, Phys. Rev. Lett. 106 (2011) 033401.
[43] M. Forstel, M. Mucke, T. Arion, A.M. Bradshaw, U. Hergenhahn, Phys. Rev. Lett. 106 (2011) 033402.
[44] I. Unger, R. Seidel, S. Thurmer, M.N. Pohl, E.F. Aziz, L.S. Cederbaum, E. Muchova, P. Slavicek, B. Winter, N.V. Kryzhevoi, Nat. Chem. 9 (2017) 708.
[45] V. Stumpf, N.V. Kryzhevoi, K. Gokhberg, L.S. Cederbaum, Phys. Rev. Lett. 112 (2014) 193001.
[46] A.C. LaForge, V. Stumpf, K. Gokhberg, J. von Vangerow, F. Stienkemeier, N.V. Kryzhevoi, P. O'Keeffe, A. Ciavardini, S.R. Krishnan, M. Coreno, K.C. Prince, R. Richter, R. Moshammer, R. Pfeifer, L.S. Cederbaum, M. Mudrich, Phys. Rev. Lett. 116 (2016) 203001.
[47] T. Hartman, P.N. Juranic, B. Collins, K.and Reilly, N. Appathurai, R. Wehlitz, Phys. Rev. Lett. 108 (2012) 023001.
[48] U. Even, I. Al-Hroub, J. Jortner, J. Chem. Phys. 115 (2001) 2069.
[49] U. Even, J. Jortner, D. Noy, N. Lavie, C. Cossart-Magos, J. Chem. Phys. 112 (2000) 8068.
[50] A. Knie, A. Hans, M. Forstel, H.U., P. Schmidt, P. Reiss, C. Ozga, B. Kambs, F. Trinter, J. Voigtsberger, D. Metz, T. Jahnke, R. Doerner, A.I. Kuleff, L.S. Cederbaum, P.V. Demekhin, A. Ehresmann, N. J. Phys. 16 (2014) 102002.
[51] A. Hans, C. Kuestner-Wetekam, P. Schmidt, C. Ozga, X. Holzapfel, H. Otto, C. Zindel, C. Richter, L.S. Cederbaum, A. Ehresmann, U. Hergenhahn, N.V. Kryzhevoi, A. Knie, Phys. Rev. Res. 2 (2020) 012022(R).